Tokyo Climate Center, Japan Meteorological Agency

# TCC News

**Autumn 2021**

## Table of Contents: TCC News No. 66



## El Niño Outlook (November 2021 - May 2022)

La Niña conditions are considered to be present in the equatorial Pacific. La Niña conditions are more likely to continue (60%) until the end of boreal winter than not (40%) (article based on the El Niño outlook issued on 10 November 2021).

### 1. El Niño/La Niña

In October 2021, the sea surface temperature (SST) for the NINO.3 region was below normal with a deviation of -0.7°C. SSTs in the equatorial Pacific were above normal in the western part and below normal in central and eastern parts (Figures 1-1 and 1-3 (a)). Subsurface temperatures were above normal in the western part and below normal in central and eastern parts (Figures 1-2 and 1-3 (b)). Atmospheric convective activity near the date line over the equatorial Pacific was below normal, and easterly winds in the lower troposphere (i.e., trade winds) over the central equatorial Pacific were stronger than normal. These oceanic and atmospheric conditions are consistent with features commonly seen in past La Niña events. La Niña conditions are considered to be present in the equatorial Pacific.

The subsurface cold waters observed in the central and eastern equatorial Pacific in October are expected to propagate eastward in the coming months and contribute to ongoing low SSTs in the eastern part. JMA's El Niño

model predicts that easterly winds over the central equatorial Pacific will remain stronger than normal during the coming winter in association with high SSTs and enhanced convective activity in the western equatorial Pacific. These atmospheric anomalies indicate a high likelihood of monthly NINO.3 SST below-0.5°C until early winter. However, the probability of NINO.3 SST satisfying JMA's definition of La Niña event (a five-month moving average below-0.5°C for six consecutive months) needs to be adjusted slightly downward to account for predicted NINO.3 SST being closer to normal toward spring (Figure 1-4). In conclusion, La Niña conditions are more likely to continue until the end of boreal winter and meet the definition (60%) than not (40%) (Figure 1-5).

## 2. Western Pacific and Indian Ocean

The area-averaged SST in the tropical western Pacific (NINO.WEST) region was above normal in October. Index values are likely to be above or near normal until boreal spring.

The area-averaged SST in the tropical Indian Ocean (IOBW) region was below normal in October. Index values are likely to be below or near normal until boreal spring.

* The SST normal for the NINO.3 region (5°S – 5°N, 150°W – 90°W) is defined as a monthly average over the latest sliding 30-year period (1991-2020 for this year).

* The SST normals for the NINO.WEST region (Eq. – 15°N, 130°E – 150°E) and the IOBW region (20°S – 20°N, 40°E – 100°E) are defined as linear extrapolations with respect to the latest sliding 30-year period, in order to remove the effects of significant long-term warming trends observed in these regions.

(a) (b)

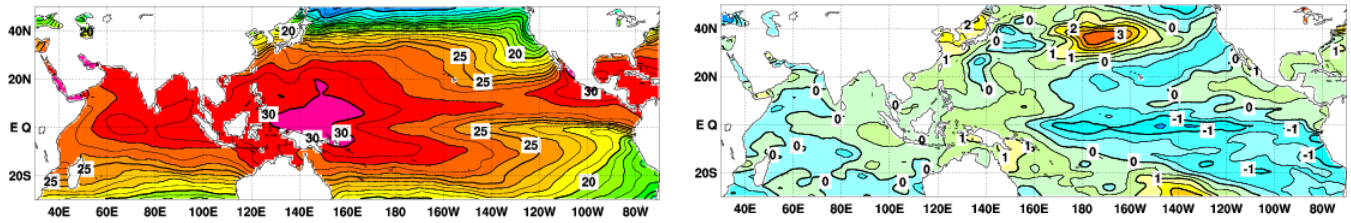


**Figure 1-1 Monthly mean (a) sea surface temperatures (SSTs) and (b) SST anomalies in the Indian and Pacific Ocean areas for October 2021**
The contour intervals are 1°C in (a) and 0.5°C in (b). The base period for the normal is 1991 – 2020.

(a) (b)

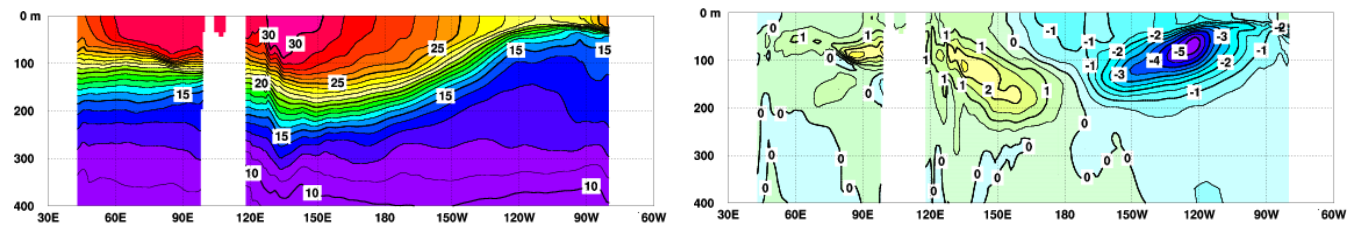


**Figure 1-2 Monthly mean depth-longitude cross sections of (a) temperatures and (b) temperature anomalies in the equatorial Indian and Pacific Ocean areas for October 2021**
The contour intervals are 1°C in (a) and 0.5°C in (b). The base period for the normal is 1991 – 2020.

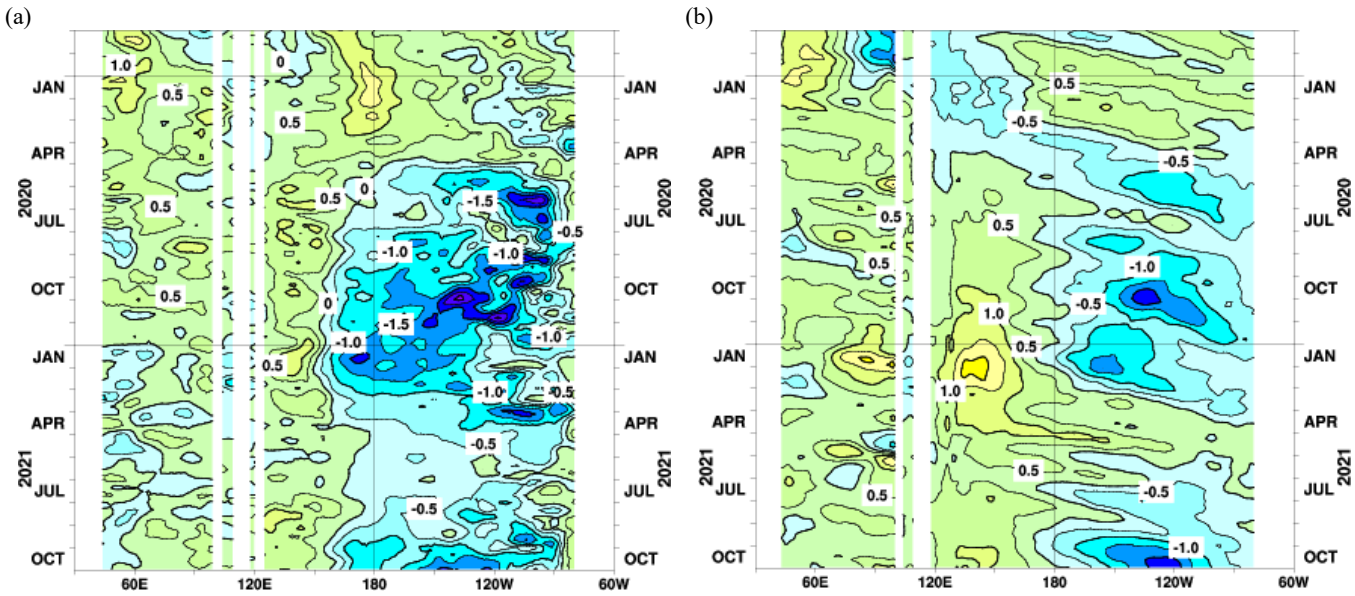


**Figure 1-3 Time-longitude cross sections of (a) SST and (b) ocean heat content (OHC) anomalies along the equator in the Indian and Pacific Ocean areas**

OHCs are defined here as vertically averaged temperatures in the top 300 m. The base period for the normal is 1991 – 2020.

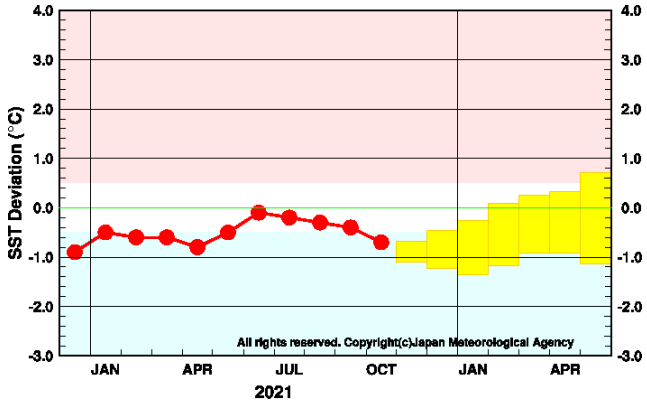


**Figure 1-4 Outlook of NINO.3 SST deviation produced by the El Niño prediction model**

This figure shows a time series of monthly NINO.3 SST deviations. The thick line with closed circles shows observed SST deviations, and the boxes show the values produced for up to six months ahead by the El Niño prediction model. Each box denotes the range into which the SST deviation is expected to fall with a probability of 70%.

| YEAR | MONTH | mean period | El Niño | ENSO neutral | La Niña |
|---|---|---|---|---|---|
| 2021 | SEP | JUL2021–NOV2021 | 10 | 90 | |
| | OCT | AUG2021–DEC2021 | 10 | 90 | |
| | **NOV** | **SEP2021–JAN2022** | 10 | 90 | |
| | **DEC** | **OCT2021–FEB2022** | 10 | 90 | |
| 2022 | **JAN** | **NOV2021–MAR2022** | 20 | 80 | |
| | **FEB** | **DEC2021–APR2022** | 40 | 60 | |
| | **MAR** | **JAN2022–MAY2022** | 60 | 40 | |

**Figure 1-5 ENSO forecast probabilities based on the El Niño prediction model**

Red, yellow and blue bars indicate probabilities that the five-month running mean of the NINO.3 SST deviation from the latest sliding 30-year mean will be +0.5°C or above (El Niño), between +0.4 and -0.4°C (ENSO-neutral) and -0.5°C or below (La Niña), respectively. Regular text indicates past months, and bold text indicates current and future months.

*(SATO Hitoshi, Tokyo Climate Center)*

<<Table of contents <Top of this article

# JMA's Seasonal Numerical Ensemble Prediction for Boreal Winter 2021/2022

This report outlines JMA's dynamical seasonal ensemble prediction for boreal winter 2021/2022 (December – February, referred to as DJF), which was used as a basis for JMA's operational three-month outlook issued on 24 November 2021. The outlook is based on the seasonal ensemble prediction system of the Coupled Atmosphere-ocean General Circulation Model (CGCM).

Summary: Based on JMA's seasonal ensemble prediction system, sea surface temperatures (SSTs) are expected to be below normal in the central-to-eastern equatorial Pacific during boreal winter 2021/2022, suggesting a continuation of La Niña conditions. In association with above-normal SSTs around the Maritime Continent, enhanced convection is expected in and around Southeast Asia, resulting in upper-tropospheric anti-cyclonic circulation anomalies over southern China and a northward meandering subtropical jet stream over the region.

## 1. Sea surface temperature

Figure 2-1 shows predicted SSTs (contours) and related anomalies (shading) for DJF. In the equatorial Pacific, negative anomalies in central-to-eastern parts and positive anomalies in the western part are expected. As subsurface ocean temperature anomalies in the eastern equatorial Pacific are expected to be negative (not shown), La Niña conditions are likely to continue during the period. Near-normal SSTs are expected over the equatorial Indian Ocean.

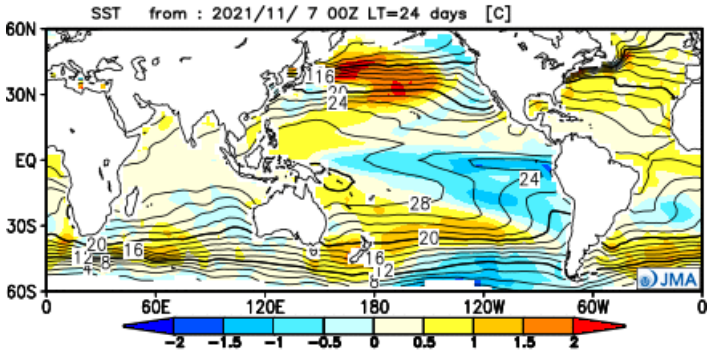


**Figure 2-1 Predicted SSTs (contours) and SST anomalies (shading) for December–February 2021/2022 (ensemble mean of 51 members)**

## 2. Prediction for the tropics and sub-tropics

Figure 2-2 (a) shows predicted precipitation (contours) and related anomalies (shading) for DJF. In association with positive SST anomalies around the Maritime Continent, above-normal precipitation is expected in and around Southeast Asia. Below-normal precipitation is expected over the western-to-central equatorial Pacific.

Figure 2-2 (b) shows predicted velocity potential (contours) and related anomalies (shading) in the upper troposphere for DJF. In association with the precipitation anomalies detailed above, negative (i.e., large-scale divergent) anomalies are expected over Southeast Asia, while positive (i.e., large-scale convergent) anomalies are expected near the date line over the equatorial Pacific.

Figure 2-2 (c) shows predicted stream functions (contours) and related anomalies (shading) in the upper troposphere for DJF. Anti-cyclonic (i.e., positive) circulation anomalies are expected over southern China, and cyclonic

(i.e., negative in the Northern Hemisphere) circulation anomalies straddling the equator are expected over the central tropical Pacific.

Figure 2-2 (d) shows predicted stream functions (contours) and related anomalies (shading) in the lower troposphere for DJF. Cyclonic (i.e., negative in the Northern Hemisphere) circulation anomalies straddling the equator are expected from the eastern tropical Indian Ocean to the Maritime Continent, and anti-cyclonic (i.e., positive in the Northern Hemisphere) circulation anomalies straddling the equator are expected near the date line in the equatorial Pacific.

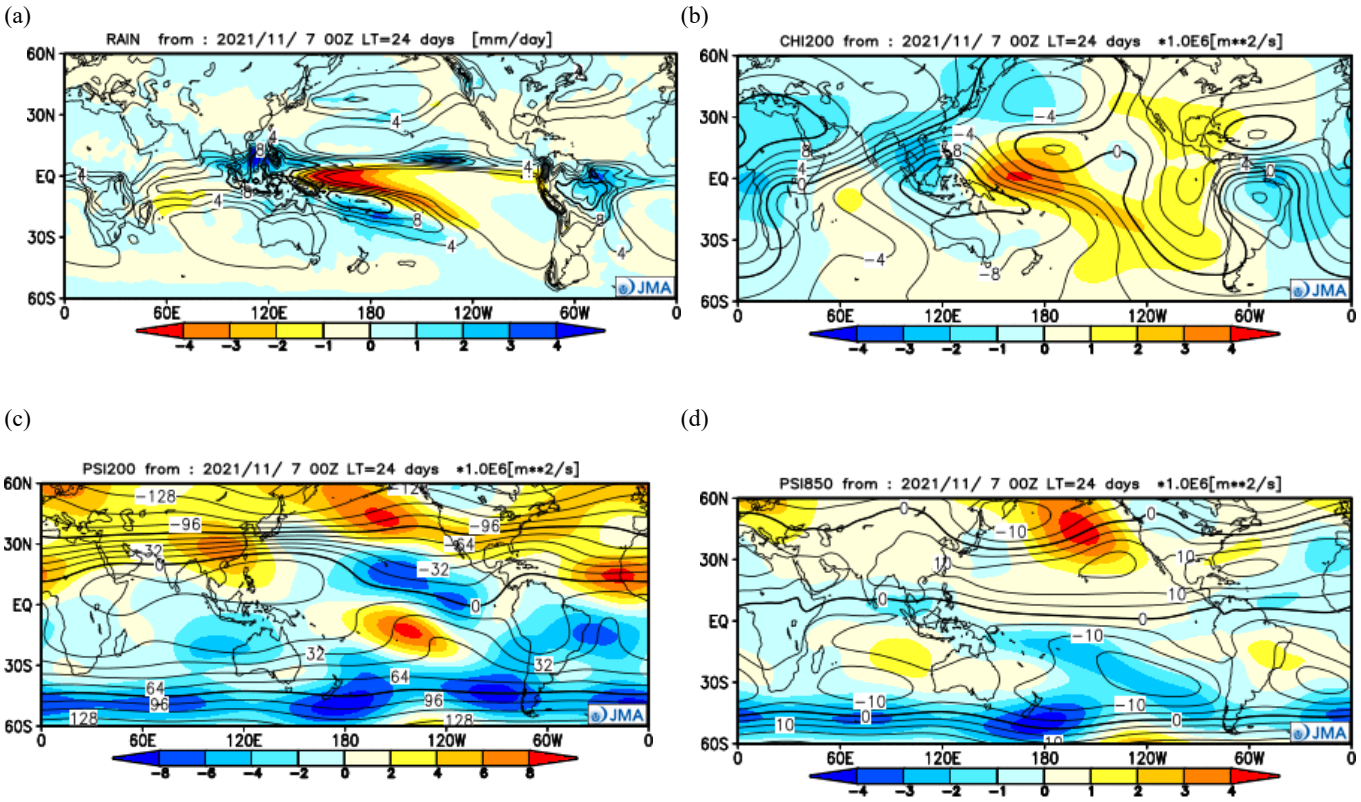


**Figure 2-2 Predicted atmospheric fields over 60°N-60°S for December-February 2021/2022 (ensemble mean of 51 members)**
(a) Precipitation (contours) and anomaly (shading). The contour interval is 2 mm/day. (b) Velocity potential at 200-hPa (contours) and anomaly (shading). The contour interval is $2 \times 10^6$ m$^2$/s. (c) Stream function at 200-hPa (contours) and anomaly (shading). The contour interval is $16 \times 10^6$ m$^2$/s. (d) Stream function at 850-hPa (contours) and anomaly (shading). The contour interval is $5 \times 10^6$ m$^2$/s.

## 3. Prediction for the mid- and high- latitudes of the Northern Hemisphere

Figure 2-3 (a) shows predicted 500-hPa geopotential heights (contours) and related anomalies (shading) for DJF. Wave trains are expected from the mid-latitude North Pacific to North America and around Europe, with positive anomalies to the southeast of the Aleutian Islands and over northern Europe, and negative anomalies over the northwestern part of North America.

Figure 2-3 (b) shows predicted sea level pressure (contours) and related anomalies (shading) for DJF. In association with 500-hPa geopotential height anomalies, the Aleutian Low is expected to shift westward of its normal position and positive sea level pressure anomalies are expected over northern Europe.

(a) (b)

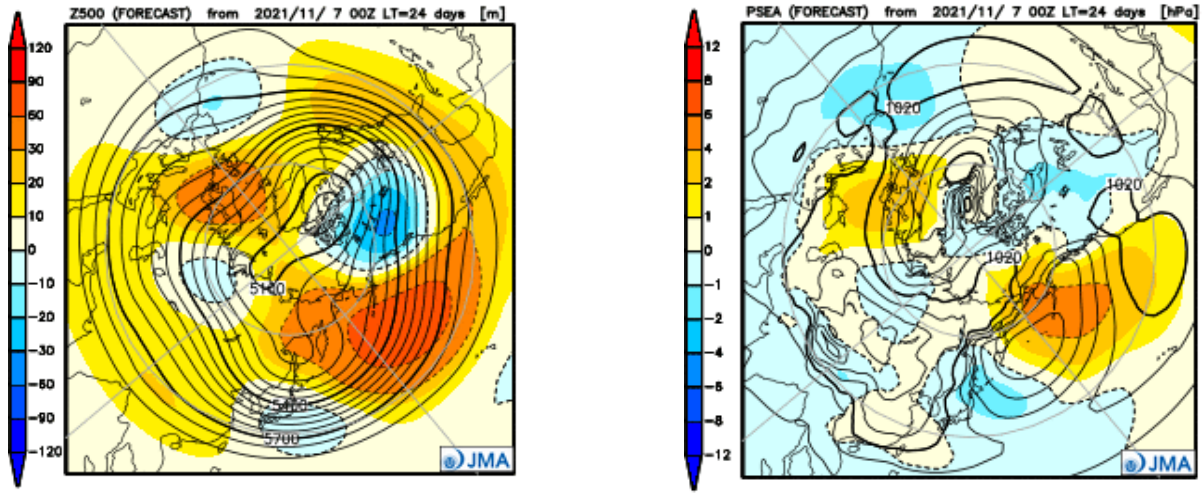


**Figure 2-3 Predicted atmospheric fields over 20°N-90°N for December-February 2021/2022 (ensemble mean of 51 members)**
(a) Geopotential height at 500-hPa (contours) and anomaly (shading). The contour interval is 60 m. (b) Sea level pressure (contours) and anomaly (shading). The contour interval is 4 hPa.

Note: JMA operates a seasonal Ensemble Prediction System (EPS) using the Coupled atmosphere-ocean General Circulation Model (CGCM) to make seasonal predictions beyond a one-month time range. The EPS produces perturbed initial conditions by means of a combination of the initial perturbation method and the lagged average forecasting (LAF) method. The prediction is made using 51 members from the latest four initial dates (13 members are run every 5 days). Details of the prediction system and verification maps based on 30-year hindcast experiments (1981–2010) are available at https://ds.data.jma.go.jp/tcc/tcc/products/model/.

*(SATO Hitoshi, Tokyo Climate Center)*

<<Table of contents <Top of this article

# Summary of the 2021 Asian Summer Monsoon

This report summarizes the characteristics of the surface climate and atmospheric/oceanographic considerations related to the Asian summer monsoon for 2021.

Note: The Japanese 55-year Reanalysis (JRA-55; Kobayashi et al. 2015) atmospheric circulation data and COBE-SST (Ishii et al. 2005) sea surface temperature (SST) data were used for this investigation. NOAA Interpolated Outgoing Longwave Radiation (OLR) data (Liebmann and Smith 1996) provided by the U.S. NOAA Earth System Research Laboratory (ESRL) from their web site at https://www.esrl.noaa.gov/psd/ was referenced to infer tropical convective activity. The base period for the normal is 1991 to 2020. The term "anomaly" as used in this report refers to deviation from the normal.

## 1. Precipitation and temperature

CLIMAT data on four-month total precipitation for the summer monsoon season (June – September) show more than 140% of the normal in central and northern East Asia, in Indonesia, and in/around southwestern Pakistan, while values less than 60% of the normal were seen in northwestern China and southwestern Central Asia (Figure 3-1 (a)). Monthly precipitation for August in western Japan was the highest on record since 1946. Heavy rain caused more than 300 fatalities in central China from mid- to late July (Chinese Government) and more than 1,000 fatalities in/around South Asia from June to August (governments of India/Pakistan/Nepal, European Commission).

Four-month mean temperatures for the same period were above normal in many parts of East and Central Asia, while values were below normal in northern East Asia and part of Southeast and South Asia (Figure 3-1 (b)). Monthly mean temperatures were the second highest for June and the third highest for July in northern Japan since 1946 (Japan Meteorological Agency) and the second highest for July in China since 1961 (China Meteorological Administration).

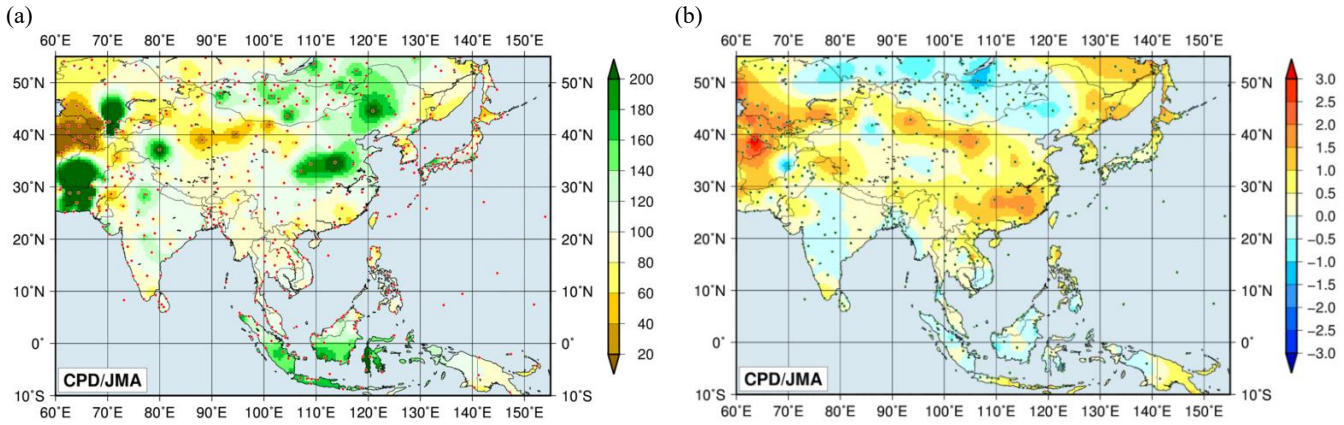


**Figure 3-1 Four-month (a) precipitation ratios [%] and (b) mean temperature anomalies [°C] from June to September 2021**
The base period for normal is 1991 – 2020. The red (a) and green (b) dots show stations providing map data, which are interpolated due to a lack of CLIMAT reporting and climatological normal values in some areas.

## 2. Tropical cyclones

A total of 16 named tropical cyclones (TCs) had formed over the western North Pacific and the South China Sea by September 2021, as compared to the normal of 18.6 (Table 3-1). From June to September, a total of 13 named TCs (climatological normal: 16.1) formed, with 10 approaching or making landfall on East Asia and 8 (climatological normal: 9.5) approaching or making landfall on Japan.

In late July, Typhoon In-Fa passed over Japan's Okinawa region with a maximum wind speed of 85 knots and made landfall on eastern China, bringing rainfall of 283.5 mm from 21st to 24th July in Naha, Japan (monthly climatological normal for July: 188.1 mm) and more than 170 mm from 24th to 27th July in Shanghai, China (monthly climatological normal for July: 144.1 mm).

**Table 3-1 Tropical cyclones reaching TS intensity or higher formed over the western North Pacific and the South China Sea by September 2021**

| Name (number) | | Date (UTC) | Category[1)] | Maximum wind[2)] (kt) |
|---|---|---|---|---|
| Dujuan | (2101) | 18 Feb - 21 Feb | TS | 40 |
| Surigae | (2102) | 13 Apr - 24 Apr | TY | 120 |
| Choi-wan | (2103) | 30 May - 5 Jun | TS | 40 |
| Koguma | (2104) | 11 Jun - 13 Jun | TS | 35 |
| Champi | (2105) | 23 Jun - 27 Jun | TY | 65 |
| In-fa | (2106) | 17 Jul - 27 Jul | TY | 85 |
| Cempaka | (2107) | 18 Jul - 21 Jul | TY | 70 |
| Nepartak | (2108) | 23 Jul - 28 Jul | TS | 40 |
| Lupit | (2109) | 4 Aug - 8 Aug | TS | 45 |
| Mirinae | (2110) | 5 Aug - 9 Aug | STS | 50 |
| Nida | (2111) | 4 Aug - 7 Aug | STS | 55 |
| Omais | (2112) | 20 Aug - 23 Aug | TS | 45 |
| Conson [3)] | (2113) | 6 Sep - 11 Sep | STS | 55 |
| Chanthu [3)] | (2114) | 7 Sep - 18 Sep | TY | 115 |
| Dianmu [3)] | (2115) | 23 Sep - 24 Sep | TS | 35 |
| Mindulle [3)] | (2116) | 23 Sep - 1 Oct | TY | 105 |

Note: Based on information from the RSMC Tokyo-Typhoon Center.
1) Intensity classification for tropical cyclones.
TS: tropical storm, STS: severe tropical storm, TY: typhoon
2) Estimated maximum 10-minute mean wind.
3) Based on early analysis data, but not best track.

## 3. Monsoon activity and atmospheric circulation

Convective activity inferred from OLR averaged for June – September 2021 (Figure 3-2) was enhanced from the southeastern tropical Indian Ocean to the Maritime Continent and over the seas south of Japan, and was suppressed over the western and northern tropical Indian Ocean, from the Indochina Peninsula to the seas east of the Philippines and over the seas east of New Guinea, in association with a negative Indian Ocean Dipole (IOD) mode episode, which is characterized by positive SST anomalies in the southeastern tropical Indian Ocean and negative SST anomalies in

the western tropical Indian Ocean, and La Niña-like SST anomalies in the equatorial Pacific (Figure 3-3). OLR index data (Table 3-2) indicate that the overall activity of the Asian summer monsoon (represented by the SAMOI (A) index) was below normal. The active convection area was shifted southward (SAMOI (N) index) and westward (SAMOI (W) index) of its normal position in May, August and September, and northward and eastward from June to July.

Figure 3-4 shows four-month mean 200- and 850-hPa stream function fields for June – September. In the upper troposphere (Figure 3-4 (a)), anti-cyclonic circulation anomalies were seen over southern Eurasia and Eastern Siberia, while cyclonic circulation anomalies were seen over the western tropical North Pacific. In the lower troposphere (Figure 3-4 (b)), cyclonic circulation anomalies straddling the equator were seen over the eastern tropical Indian Ocean, while anti-cyclonic circulation anomalies straddling the equator were seen over the western tropical Pacific. The North Pacific Subtropical High (NPSH) extended southwestward of its climatological extent, and the monsoon trough over Southeast Asia was weaker than normal. Such lower-tropospheric circulation anomalies over tropical Indo-western Pacific Ocean areas were associated with the local convection anomalies described above. In association with the upper-tropospheric ridge over Eastern Siberia, lower-tropospheric anti-cyclonic circulation anomalies were prominent over the area from Eastern Siberia to northern Japan.

In contrast to weaker-than-normal average Asian monsoon activity during summer, convective activity in the region exhibited remarkable intraseasonal fluctuations. Values over India and the Bay of Bengal (Figure 3-5 (a)) were enhanced in the latter half of May, mid-June, mid-August and September, and were suppressed from late June to early July and from the end of July to early August. Convective activity over the Philippines (Figure 3-5 (b)) was enhanced in early June, the latter half of July and early October, and was suppressed in May, mid-August and mid-September. These fluctuations generally corresponded to large-amplitude boreal summer intraseasonal oscillation (BSISO; Lee et al. 2013).

In particular, significant changes in atmospheric conditions were observed from July to August. From the latter half of July to the beginning of August, convective activity was enhanced over the seas south of Japan in association with a stronger-than-normal monsoon trough (not shown). Conditions changed in August, when areas from western to eastern Japan experienced record-heavy rain. A stationary front was strengthened by a significant north-south gradient of temperature in the lower troposphere between the Okhotsk High to the north of Japan and a southward-shifted NPSH expanding to the south of Japan (Figure 3-6 (c)). A continuous confluence of water vapor from continental China and along the margin of the NPSH also contributed to widespread continuous heavy rainfall. The southward shift of the NPSH was related to an overall southward shift of the subtropical jet stream (STJ) over East Asia in the upper troposphere (Figure 3-6 (b)) and suppressed convection over the western tropical North Pacific (Figure 3-6 (a)) in association with phasal transition of the BSISO. The southward shift of the STJ was likely affected by SST anomalies accompanying negative IOD conditions (see also Figure 3-3) and related suppressed convection over the Asian summer monsoon region (Figure 3-6 (a)). A significant southward meandering of the STJ to the west of Japan is considered to have produced favorable conditions for updraft occurrence and persistent rainfall from western to eastern Japan.

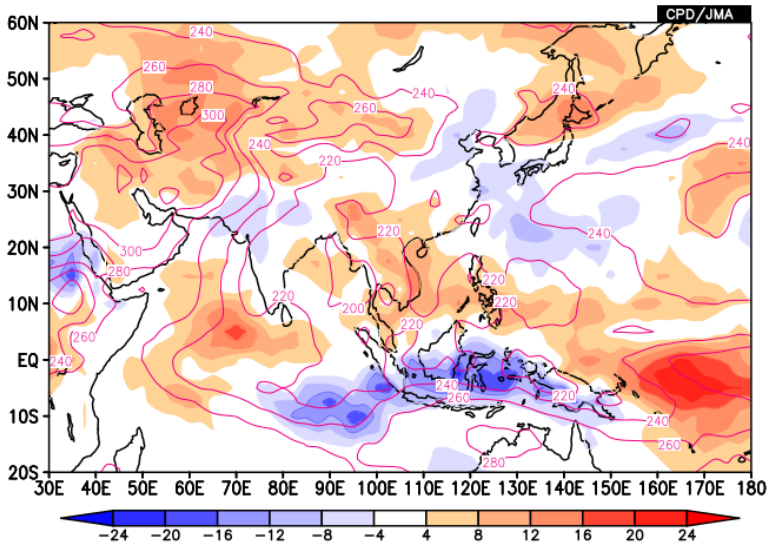


**Figure 3-2 Four-month mean OLR [W/m$^2$] for June–September 2021**
Contours indicate OLR at intervals of 20 W/m$^2$, and color shading denotes OLR anomalies from the normal (i.e., the 1991–2020 average). Negative (cold color) and positive (warm color) OLR anomalies show enhanced and suppressed convection compared to the normal, respectively.

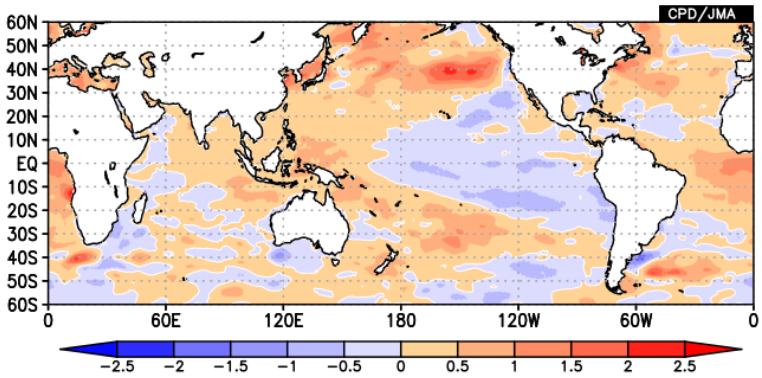


**Figure 3-3 Four-month mean SST anomalies [°C] for June–September 2021**
The base period for the normal is 1991 – 2020.

**Table 3-2 Summer Asian Monsoon OLR Index (SAMOI) values observed from May to September 2021**
Asian summer monsoon OLR indices (SAMOI) are derived from OLR anomalies. SAMOI (A), (N) and (W) indicate the overall activity of the Asian summer monsoon, its northward shift and its westward shift, respectively. SAMOI definitions are as follows: SAMOI (A) = (-1) × (W + E); SAMOI (N) = S – N; SAMOI (W) = E – W. W, E, N and S indicate area-averaged OLR anomalies for the respective regions shown in the figure on the right normalized by their standard deviations.

| | Summer Asian Monsoon OLR Index (SAMOI) | | |
|---|---|---|---|
| | SAMOI (A): Activity | SAMOI (N): Northward-shift | SAMOI (W): Westward-shift |
| May 2021 | -0.7 | -2.2 | +0.4 |
| Jun 2021 | -1.5 | +2.1 | -0.5 |
| Jul 2021 | -0.6 | +0.2 | -1.8 |
| Aug 2021 | -1.6 | -0.7 | +0.5 |
| Sep 2021 | -0.1 | -0.2 | +0.7 |

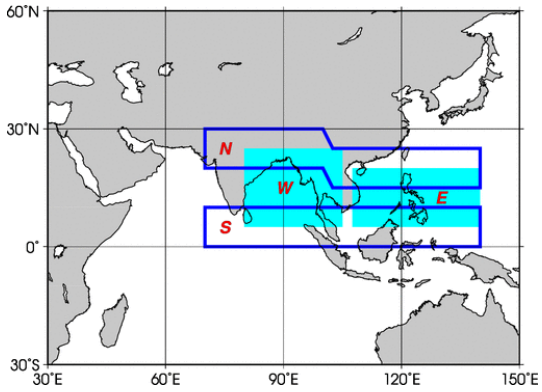

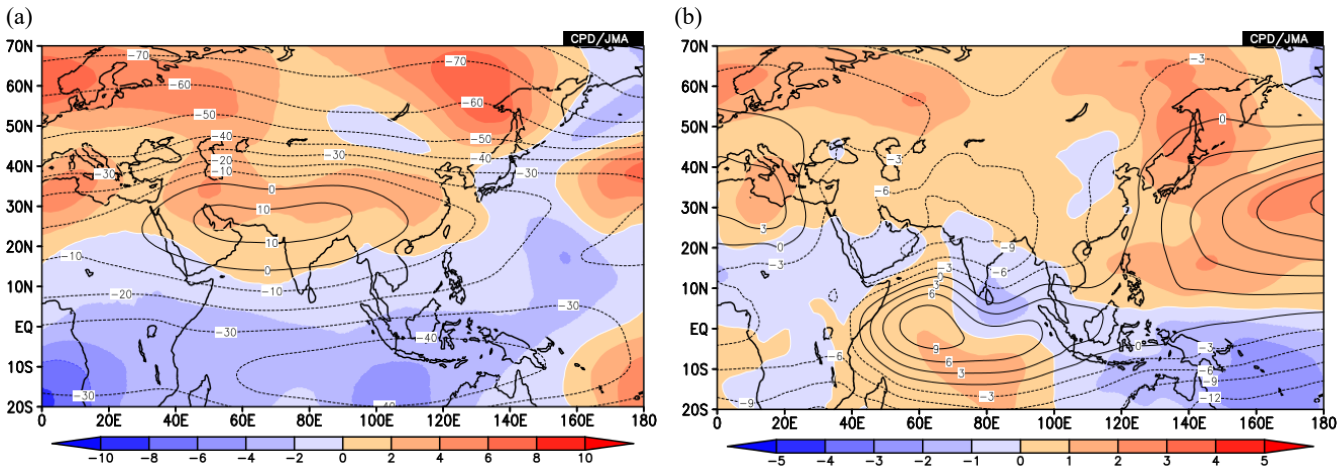


**Figure 3-4 Four-month mean (a) 200-hPa and (b) 850-hPa stream function [$10^6$ $m^2/s$] for June–September 2021**
Contours indicate stream function at intervals of (a) $10 \times 10^6$ $m^2/s$ and (b) $3 \times 10^6$ $m^2/s$, and shading shows stream function anomalies. Red (blue) shading denotes anti-cyclonic (cyclonic) circulation anomalies in the Northern Hemisphere, and vice-versa in the Southern Hemisphere. The base period for the normal is 1991 – 2020.

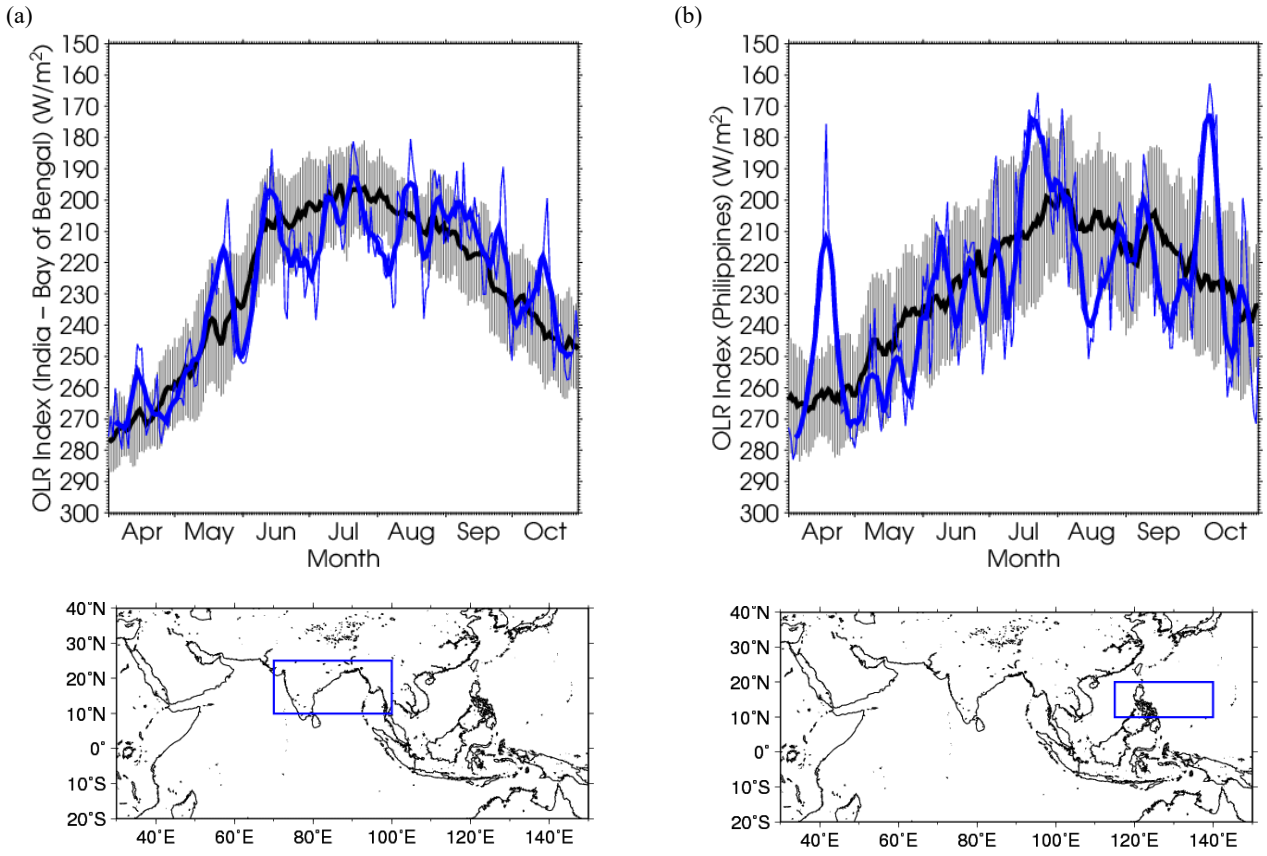


**Figure 3-5 Time-series representation of OLR [$W/m^2$] averaged over (a) India and the Bay of Bengal (shown by the rectangle on the bottom: 10°N - 25°N, 70°E - 100°E) and (b) the Philippines (shown by the rectangle on the bottom: 10°N - 20°N, 115°E - 140°E)**
The OLR indices are calculated after Wang and Fan (1999). The thick and thin blue lines indicate seven-day running mean and daily mean values, respectively. The black line denotes the normal (i.e., the 1991 - 2020 average), and the gray shading shows the range of the standard deviation calculated for the time period of the normal.

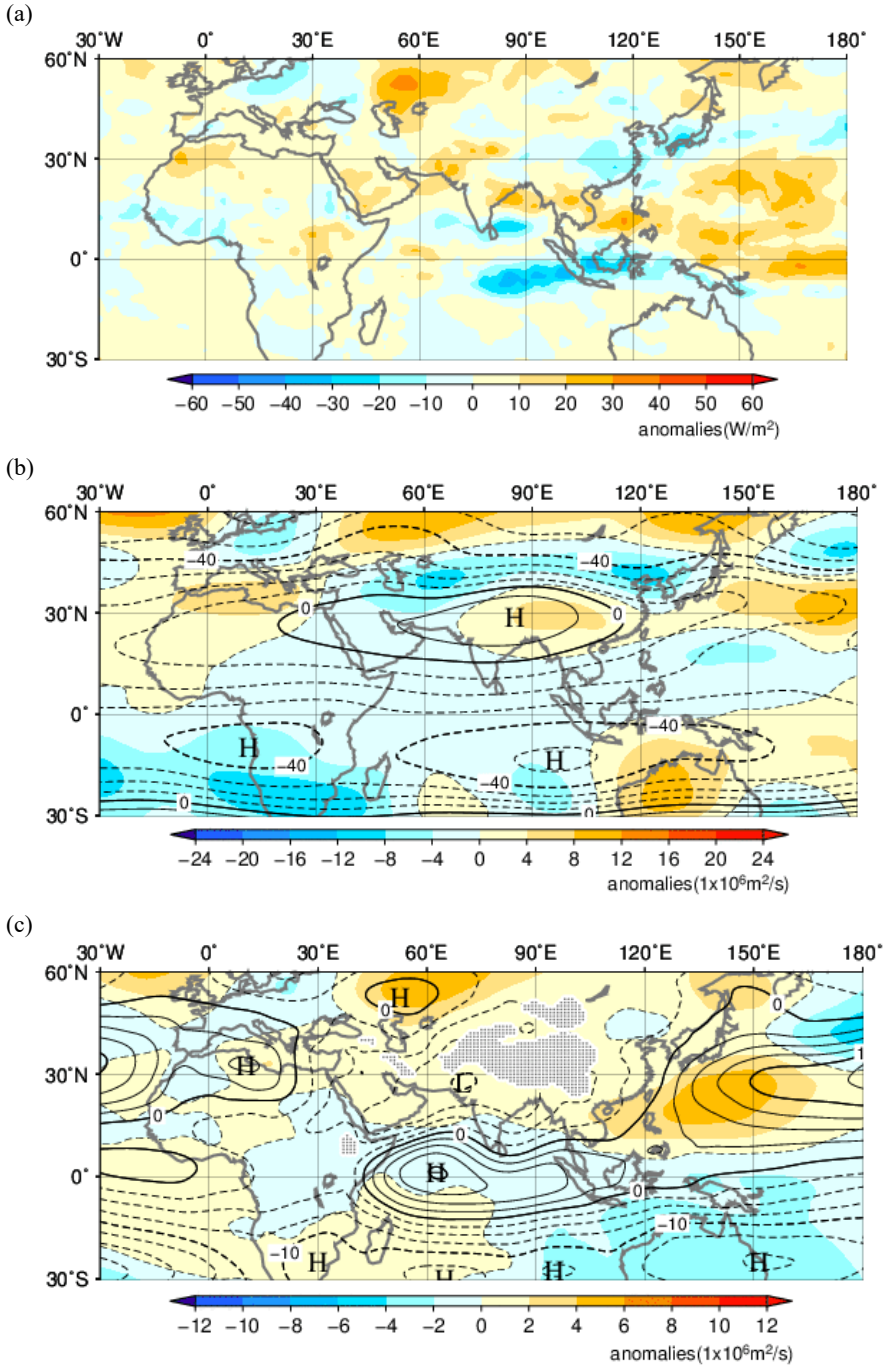


**Figure 3-6 Monthly mean (a) OLR anomalies [W/m$^2$], (b) 200-hPa stream function [$10^6$ m$^2$/s] and (c) 850-hPa stream function [$10^6$ m$^2$/s] for August 2021**

Shading indicates anomalies, and contours show stream function at intervals of (b) $10 \times 10^6$ m$^2$/s and (c) $2.5 \times 10^6$ m$^2$/s. Hatch patterns indicate areas with altitudes exceeding 1,600 m. The base period for the normal is 1991 – 2020.

## References


Ishii, M., A. Shouji, S. Sugimoto, and T. Matsumoto, 2005: Objective analyses of sea-surface temperature and marine meteorological variables for the 20th century using ICOADS and the Kobe Collection. *Int. J. Climatol.*, **25**, 865-879.

Kobayashi, S., Y. Ota, Y. Harada, A. Ebita, M. Moriya, H. Onoda, K. Onogi, H. Kamahori, C. Kobayashi, H. Endo, K. Miyaoka, and K. Takahashi, 2015: The JRA-55 Reanalysis: General specifications and basic characteristics. *J. Meteor. Soc. Japan*,

**93**, 5 – 48.

Lee, J.-Y., B. Wang, M. C. Wheeler, X. Fu, D. E. Waliser, and I.-S. Kang, 2013: Real-time multivariate indices for the boreal summer intraseasonal oscillation over the Asian summer monsoon region. *Clim. Dyn.*, **40**, 493-509.

Liebmann, B., and C. A. Smith, 1996: Description of a complete (interpolated) outgoing longwave radiation dataset. *Bull. Amer. Meteor. Soc.*, **77**, 1275–1277.

Wang, B. and Z. Fan, 1999: Choice of South Asian summer monsoon indices. *Bull. Amer. Meteor. Soc.*, **80**, 629–638.

*(SATO Hitoshi, Tokyo Climate Center)*

<<Table of contents <Top of this article

## Climate characteristics and factors behind record-heavy rain in Japan in August 2021

TCC issued a press release regarding climate characteristics of Record-heavy Rain in Japan in August 2021. An abstract of the press release and the download link for the full article are as follows.

- In mid-August 2021, areas from western to eastern Japan experienced record-heavy rain.
- The conditions observed are mainly attributed to the following:
  - Unusually for mid-summer in eastern and western Japan, like atmospheric flow in the latter half of the early-summer rainy season, known as the Baiu, a stationary front was strengthened by a significant north-south gradient of temperature in the lower troposphere between the Okhotsk High to north of Japan and the southward shifted North Pacific Subtropical High (NPSH) expanding to the south of Japan. A continuous confluence of water vapor from continental China and along the margin of the NPSH also contributed to widespread continuous heavy rainfall.
  - The southward shift of the NPSH that caused a large amount of water vapor flow into western and eastern Japan was related to the subtropical jet stream (STJ) in the upper troposphere, with an overall southward shift over East Asia. Furthermore, significant southward meandering of STJ to the west of Japan is considered to produce a favorable conditions for updraft occurrence and persistent rainfall.
  - The southward shift of the STJ was likely affected by sea surface temperatures (SSTs) in the tropical Indian Ocean and related convective activity over the Asian summer monsoon region.
- On 14th August, the northern part of the Kyushu region experienced extremely heavy rainfall associated with stationary linear mesoscale convective systems. In addition to the formation of conditions conducive to convective cloud development to the south of the front a small-scale low was also developed on the same day on the front over the East China Sea. This may have contributed to the formation of cumulonimbus clouds organized as stationary linear mesoscale convective systems over sea areas west of the Kyushu region to the east of the small-scale low.

URL: https://ds.data.jma.go.jp/tcc/tcc/news/press_20210924.pdf

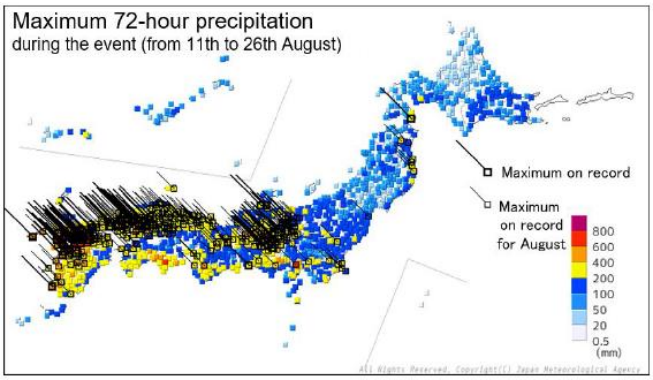


**Figure 4-1 Maximum 72-hour precipitation [mm] for 11– 26 August, 2021**

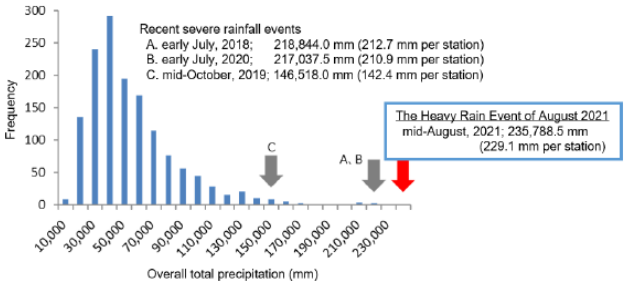


**Figure 4-2 Frequency distribution of overall total precipitation at 1029 selected AMeDAS stations throughout Japan for 10-day periods starting on the 1st, 11th and 21st of the month since 1982**

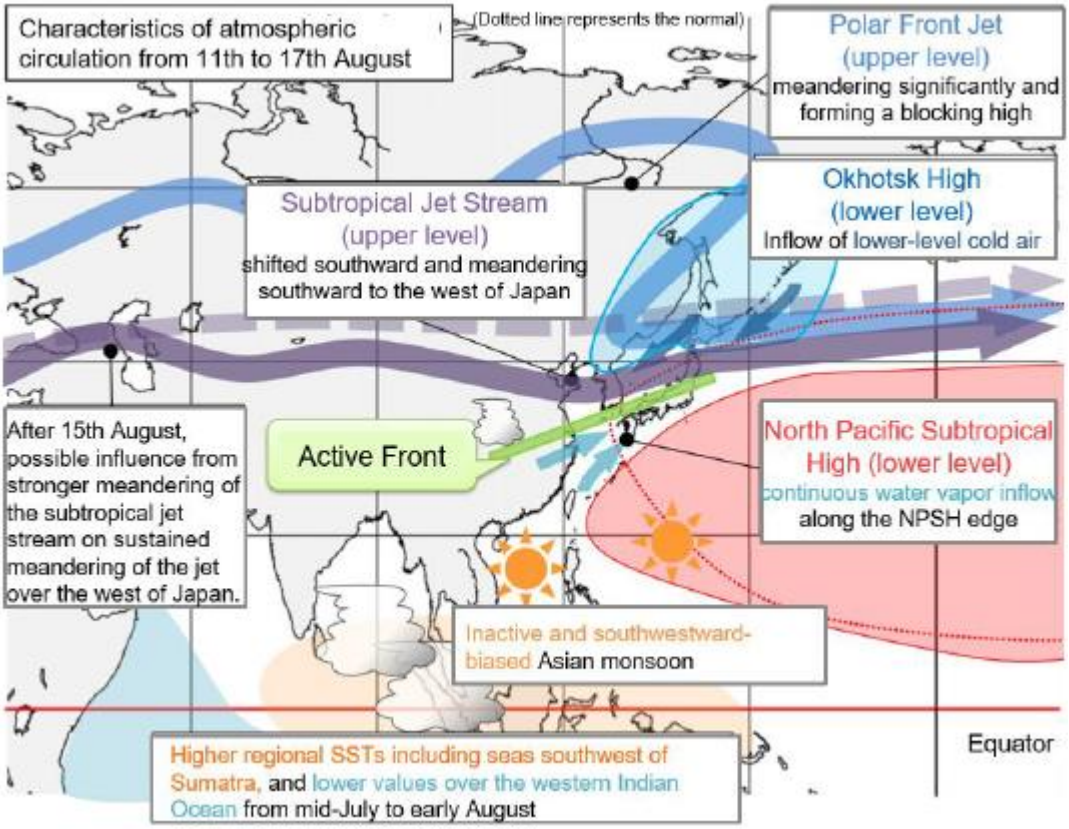


**Figure 4-3 Characteristics of atmospheric circulation bringing record-heavy rain from 11th to 17th August**

*(WAKAMATSU Shunya, Tokyo Climate Center)*


<<Table of contents <Top of this article

## Status of the Antarctic Ozone Hole in 2021

**The size of the Antarctic ozone hole in 2021 exceeded the most recent decadal average due to a large low-temperature area in the stratosphere as in 2020. Over the long term, however, a statistically significant decreasing trend in the annual maximum size has been observed since 2000.**

Since the early 1980s, the Antarctic stratospheric ozone level has fallen every year in austral spring with a peak in September or early October. This area of depletion is referred to as the Antarctic ozone hole.

JMA analysis based on data from the Ozone Mapper Profiler Suite (OMPS) aboard the Suomi National Polar-orbiting Partnership (NPP) satellite indicates that the 2021 Antarctic ozone hole appeared in early August and expanded rapidly from late August onward, exceeding the scale of the most recent decadal average (Figure 5, upper left). Its annual maximum size (observed on 7th October) was 24.8 million square kilometers (Figure 5, upper right), which is close to that observed in 2020 and about around 1.8 times as large as the Antarctic itself. In 2021 the polar vortex over Antarctica was also stable and dominant similar to that of 2020, and the low-temperature area in the stratosphere was larger than the most recent decadal average after mid-June. These conditions contributed to the year's expanded Antarctic ozone hole via increased formation of polar stratospheric clouds (PSCs), which play an important role in ozone depletion.

As an overall trend, the annual maximum size of the Antarctic ozone hole has shown a statistically significant decrease since 2000. The *WMO/UNEP Scientific Assessment of Ozone Depletion: 2018* report detailed how the hole is expected to close gradually, with springtime total column ozone in the 2060s returning to 1980 values.

The ozone layer acts as a shield against ultraviolet radiation, which can cause skin cancer. The Antarctic ozone hole was first recognized in the early 1980s, and large-scale events have been observed since the 1990s. Its record size was 29.8 million square kilometers (2000). The Antarctic ozone hole significantly affects summer climatic conditions on the surface of the Southern Hemisphere according to the recent assessment.

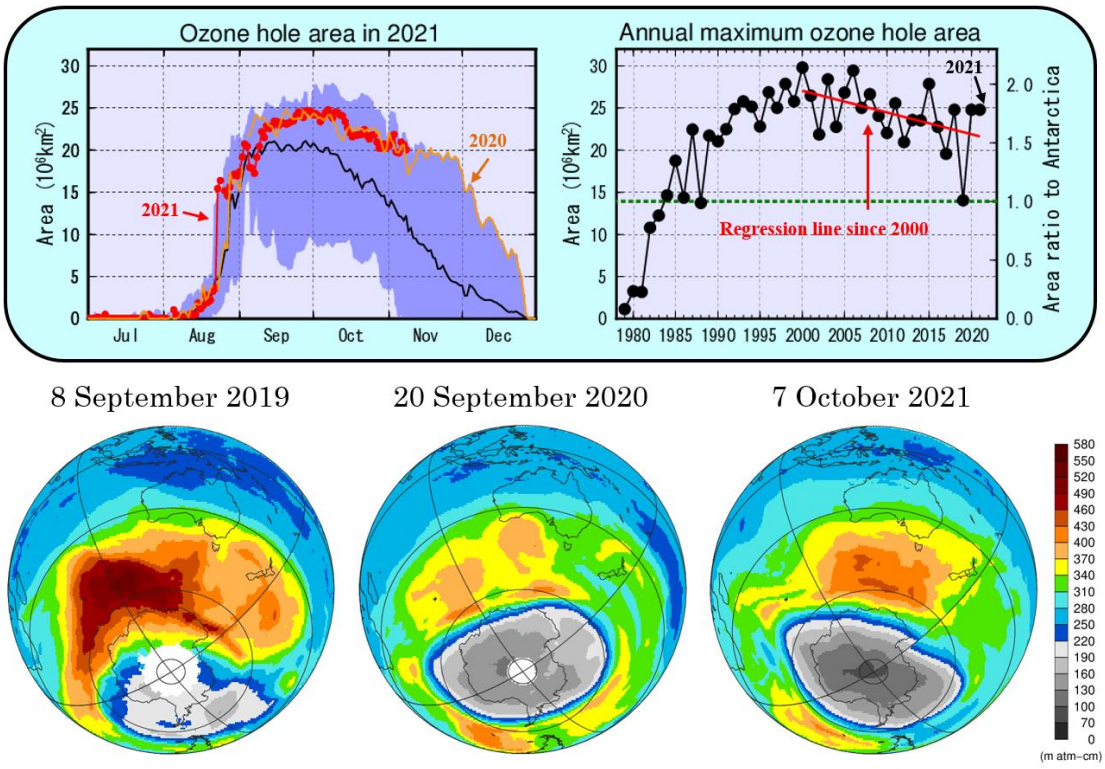


**Figure 5 The Antarctic ozone hole characteristics**

Upper left: Time-series representation of the daily ozone hole area for 2021 (red line), 2020 (orange line) and the 2011 – 2020 average (black line). Blue shading represents the range of daily maxima and minima over the previous 10 years. JMA defines the extent of Antarctic ozone hole expansion as the area in which the total ozone column value is less than or equal to 220 m atm-cm.

Upper right: Inter-annual variability of the annual maximum ozone hole area. The green dotted line shows the area of the Antarctic Continent (13.9 million square kilometers).

Bottom: Snapshots of total column ozone distribution on the day of the annual maximum ozone hole area for the previous three years; the Antarctic ozone hole is shown in grey. Images are based on NASA satellite data.

*(UEMURA Keiko, Atmospheric Environment and Ocean Division)*

<<Table of contents <Top of this article

## Status of the Arctic Sea Ice in 2021

It is virtually certain that there has been a long-term decreasing trend of sea ice extent in the Arctic Ocean since 1979, when ongoing monitoring using similar satellite sensors began (statistically significant at a confidence level of 99%). The reduction in the annual minimum extent is particularly notable at 0.089 × $10^6$ $km^2$ per year up to 2021 (Figure 6-1).

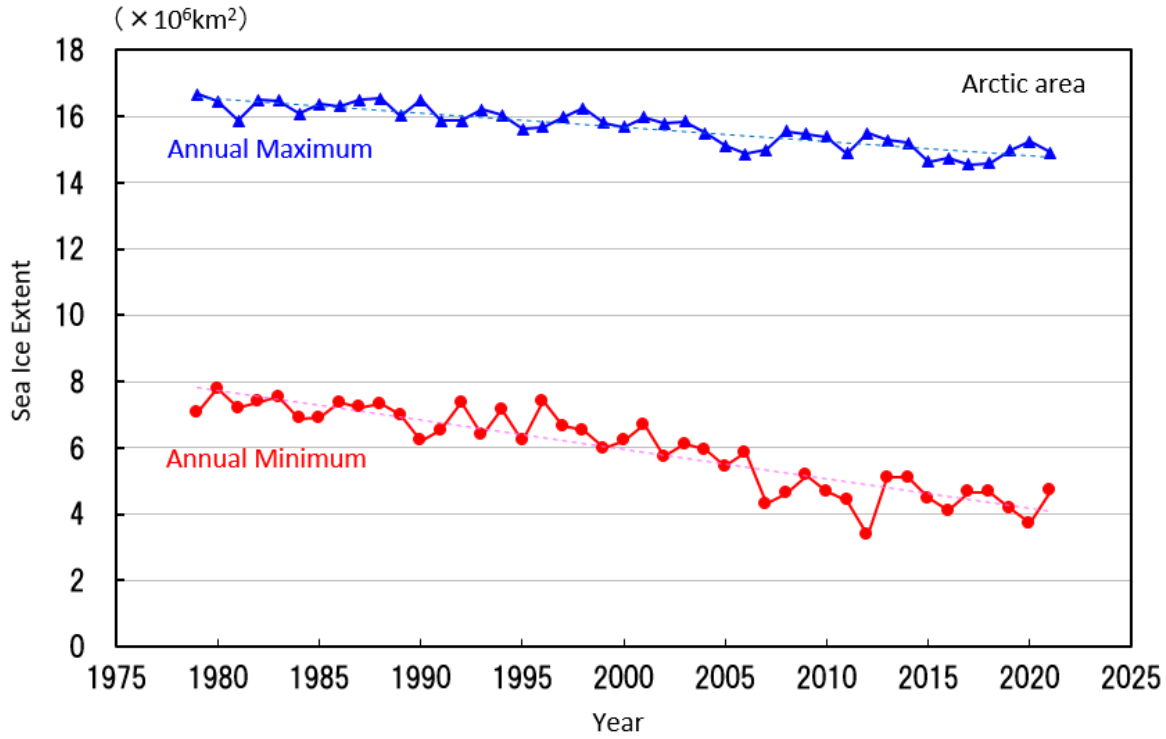


**Figure 6-1 Time-series representations of annual maximum and annual minimum sea ice extent in the Arctic Ocean (including the Sea of Okhotsk and the Bering Sea) from 1979 to 2021**
Blue and red lines indicate annual maximum and annual minimum sea ice extents, respectively, with dashed lines indicating linear trends. Sea ice extents are calculated from brightness temperature data provided by NASA (the National Aeronautics and Space Administration) and NSIDC (the National Snow and Ice Data Center).

On 8 March 2021, the preliminary annual maximum Arctic sea ice extent was 14.91 × $10^6$ $km^2$, marking the 7th-lowest value since 1979. The value subsequently decreased during spring and summer in the Northern Hemisphere and reached its annual minimum of 4.71 × $10^6$ $km^2$ on 11th September, marking the 12th-lowest level since 1979 (Figure 6-2, 6-3).

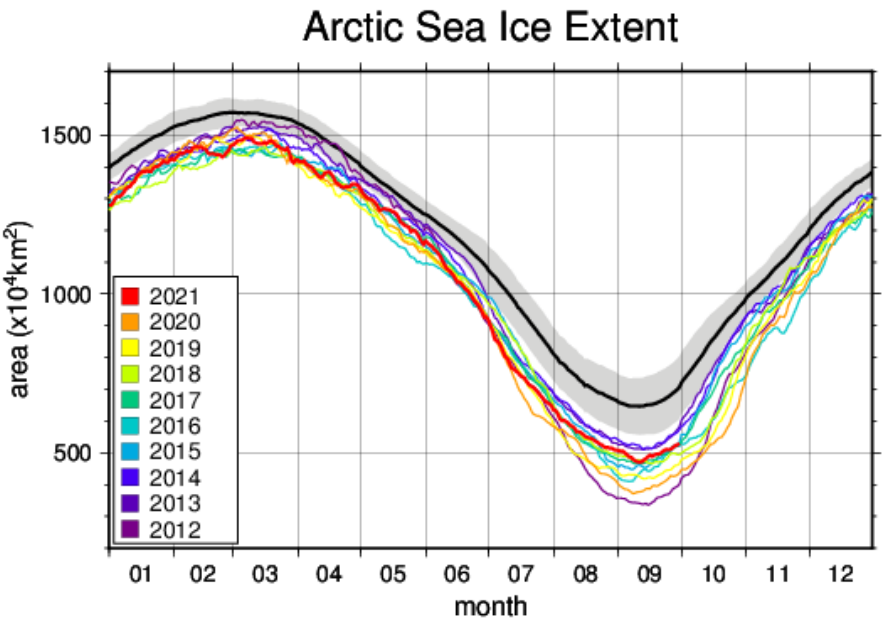


**Figure 6-2 Annual variations in the Arctic sea ice extent**
The black lines represents the normal, and shading represents the normal range. The base period for the normal is 1981 – 2010.

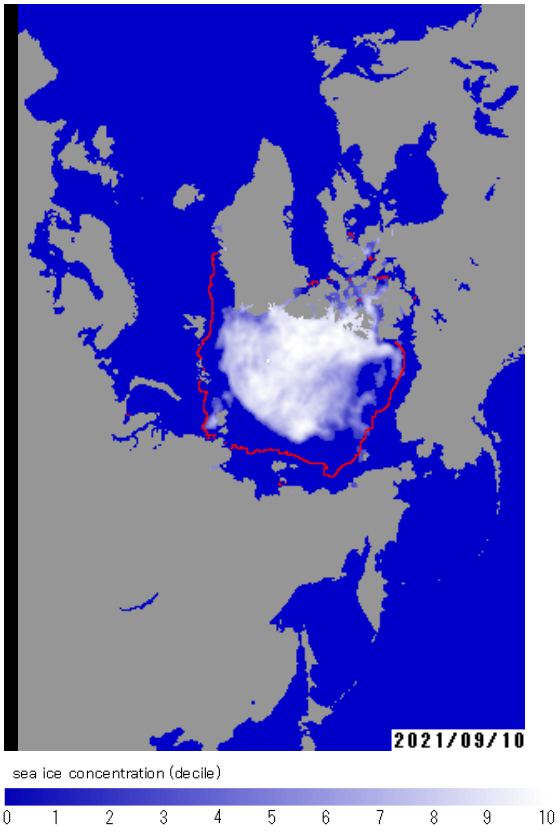


**Figure 6-3 Annual minimum Arctic sea ice distribution**
As of 10 September 2021. The red lines represents the normal extent. The base period for the normal is 1981 – 2010.

*(ADACHI Noriyuki, Office of Marine Prediction)*

<<Table of contents <Top of this article

# TCC and WMC Tokyo co-contributions to Regional Climate Outlook Forums

WMO Regional Climate Outlook Forums (RCOFs) bring together national, regional and international climate experts on an operational basis to produce regional climate outlooks based on input from participating NMHSs, regional institutions, Regional Climate Centres (RCCs) and global producers of climate predictions. By providing a platform for countries with similar climatological characteristics to discuss related matters, these forums ensure consistency in terms of access to and interpretation of climate information.

In autumn 2021, TCC representatives gave presentations at an RCOF as outlined below.

- 9th East Asia winter Climate Outlook Forum (EASCOF-9)

EASCOF-9 was hosted online by the Korea Meteorological Administration (KMA) on 4 November 2021 as a platform for summarization of the winter consensus outlook for East Asia. At the event, dozens of attendees from NMHSs and related centers in East Asia (including the China Meteorological Administration (CMA), the Japan Meteorological Agency (JMA), the National Agency for Meteorology and Environment Monitoring of Mongolia (NAMEM), the Korea Meteorological Administration (KMA), the APEC Climate Center (APCC) and the WMO Lead Centre for the Long-Range Forecast Multi-Model Ensemble (LC LRFMME)) discussed expertise and technical information relating to the East Asia monsoon. The TCC representatives gave presentations on recent operational activities, climate characteristics and factors behind the record-heavy rain observed in eastern and western Japan in August 2021, and the East Asia outlook for winter 2021/2022, which can be referenced online at https://ds.data.jma.go.jp/tcc/tcc/library/EASCOF/2021/index.html.

Representatives from TCC and the World Meteorological Centre (WMC) Tokyo also attended:

- The 20th winter session of the South Asian Climate Outlook Forum (SASCOF-20)
- The 17th session of the ASEAN Climate Outlook Forum (ASEANCOF-17)

These forums were also held online due to the COVID-19 pandemic. As part of collaborative activities between TCC and WMC Tokyo, the representatives from TCC and WMC Tokyo provided winter outlooks based on climate monitoring and forecast products from the TCC website along with an outline of plans to upgrade JMA's seasonal prediction system. The presenters also highlighted Copernicus Climate Change Service (C3S) multi-model ensemble prediction incorporating JMA's seasonal prediction system. These activities are intended to support the output of country-scale outlooks by National Meteorological and Hydrological Services (NMHSs), contribute to the summarization of consensus outlooks and reduce climate disaster risks in the water, agriculture and health sectors for each target area. TCC and WMC Tokyo are committed to collaboration with operational climate communities to enhance progress in forecast skill and application of climate information toward the resolution of common issues and realizing a climate-resilient world.

*(WAKAMATSU Shunya, Tokyo Climate Center)*

<<Table of contents <Top of this article

## TCC contributions to the Report on the States of the Climate in Asia 2020

WMO's State of the Climate in Asia 2020 report of 26 October 2021 represents a landmark collaborative effort incorporating expertise across a wide range of disciplines in the areas of climate, socio-economics and policy development. The content summarizes climate and extreme-weather events as well as related local socio-economic impacts for 2020. TCC made a significant contribution to the report in a drafting and team leadership role.

Multi-agency efforts are essential in tackling the cascading effects of climate change over a wide spectrum of disciplines, and this annual report represents the results of such collaborative work in Asia. Ongoing collaboration among Members and RCCs in RA II is expected to support future reporting in this field for the Asian region.

*(GOTO Atsushi, KAKIHARA Koichiro and WAKAMATSU Shunya, Tokyo Climate Center)*

<<Table of contents <Top of this article

You can also find the latest newsletter from Japan International Cooperation Agency (JICA).

**JICA Magazine**

https://jicamagazine.jica.go.jp/en/

"JICA Magazine" is a public relations magazine published by JICA. It introduces the current situation of developing countries around the world, the people who are active in the field, and the content of their activities.

Any comments or inquiry on this newsletter and/or the TCC website would be much appreciated.
Please e-mail to tcc@met.kishou.go.jp.
(Editors: KAKIHARA Koichiro and WAKAMATSU Shunya)

Tokyo Climate Center, Japan Meteorological Agency
3-6-9 Toranomon, Minato City, Tokyo 105-8431, Japan

TCC Website:
https://ds.data.jma.go.jp/tcc/tcc/index.html

<<Table of contents